International Journal of Control, Automation, and Systems 20(9) (2022) 2948-2958
http://dx.doi.org/10.1007/s12555-021-0105-1
ISSN:1598-6446 eISSN:2005-4092
http://www.springer.com/12555

Nonlinear Cascade Control for a New Coaxial Tilt-rotor UAV

Shengming Li , Zongyang Lv , Lin Feng, Yuhu Wu , and Yingshun Li*

Abstract: This paper proposes a nonlinear control strategy for a newly-designed coaxial tilt-rotor (CTR) unmanned aerial vehicle (UAV), which is a special class of tilt-rotor (TR) UAVs with two pairs of coaxial rotors, two servos, and a rear rotor. The CTRUAV is an underactuated system, and the controller is designed in cascade form. The proposed controller includes two sub-controllers: an inner-loop attitude controller and an outer-loop velocity controller. Each sub-controller is proposed by using a backstepping-like feedback linearization method to control and stabilize the CTRUAV. The developed control strategy can realize the motion control for the CTRUAV. The asymptotic stability of the resulting closed-loop system is analyzed by the Lyapunov method. Finally, simulations and real flight tests are performed to validate the effectiveness of the proposed control system.

Keywords: Cascade control, coaxial rotors, tilt rotor, unmanned aerial vehicle (UAV).

1. INTRODUCTION

Recently, the unmanned aerial vehicles (UAVs) have attracted tremendous interests in the research field. Various UAVs have been utilized in different missions, including aerial photography, power line maintenance, plant protection, law enforcement, transportation, and surveillance in disasters [1–5]. As a special kind of UAVs, different from other UAVs like fixed-wing UAVs and quadrotor UAVs, the tilt-rotor UAVs (TRUAVs) are mainly classified as follows: the V-22 UAV which includes two tiltable rotors with variable blade pitch [6,7], the tilt-rotor UAV which includes two tiltable rotors with fixed blade pitch [8,9], the tilt tri-rotor UAV with two tiltable rotors and one rear rotor [10,11], and the V-44 UAV with four tiltable rotors [4]. Owing to the tiltable ability of the rotors, TRUAVs can perform low-speed maneuver, take off and land vertically like quadrotor UAVs, and move horizontally at a fast speed [4,7].

Considering the advantages mentioned above, various researches have been carried out on the control design for the TRUAVs. Ta *et al*. [11] proposed a nonlinear controller whose parameters were tuned by a neural network to control the attitude and altitude of a tilt tri-rotor UAV.

Lv *et al*. [12] designed a coaxial tilt-rotor UAV and developed an adaptive controller to realize motion control for the UAV in the presence of external disturbance. However, it can only theoretically guarantees that the attitude subloop system, velocity subloop system and the whole resulting closed-loop system are asymptotically stable. Papachristos and Tzes [13] used a PID controller to control a newly designed tilt tri-rotor UAV. In research [14], Sridhar *et al*. designed a nonlinear controller to hover a tilt-rotor quadrotor at any desired orientation. Amato *et al*. [10] designed a dynamic inversion based controller to achieve robust stability for a small scale tilt tri-rotor UAV in the presence of model uncertainties. Xian and Hao [15] proposed a fault-tolerant control strategy to deal with the rear servo's fault and exogenous disturbances on a tilt tri-rotor UAV. Raffo *et al*. [8] developed a H_2/H_∞ controller to realize path tracking for the UAV with two tiltable rotors . Chowdhury *et al*. [16] designed a backstepping based PD controller to enable the tilt-rotor UAV to hover in one specific position.

To the best of our knowledge, in the research field, although various controllers have been proposed for various TRUAVs as mentioned above, the research concerning the control problem of the coaxial tilt-rotor UAV (CTRUAV), which consists of two coaxial-rotors whose axes can be tilted by servos, and one rear rotor, as shown in Fig. 1, is limited. The CTR scheme is a practical solution and has been successfully used in various aircrafts like Air-

Manuscript received February 6, 2021; revised August 11, 2021 and October 11, 2021; accepted November 25, 2021. Recommended by Associate Editor Jun Cheng under the direction of Editor Hyo-Sun Ahn. This work was supported in part by the National Natural Science Foundation of China under Grants 61773090 and 61773086, in part by Liao Ning Revitalization Talents Program under Grant XLYC1907100.

Shengming Li and Lin Feng are with School of Innovation and Entrepreneurship, Dalian University of Technology, Dalian 116024, China (e-mails: lishengming@dlut.edu.cn, fenglin@dlut.edu.cn). Zongyang Lv is with the Key Laboratory of Intelligent Control and Optimization for Industrial Equipment of Ministry of Education, and Information and Communication Engineering, Dalian University of Technology, Dalian 116024, China (e-mail: zongyanglv@dlut.edu.cn). Yuhu Wu and Yingshun Li are with the Key Laboratory of Intelligent Control and Optimization for Industrial Equipment of Ministry of Education, and School of Control Science and Engineering, Dalian University of Technology, Dalian 116024, China (e-mails: wuyuhu@dlut.edu.cn, leeys@dlut.edu.cn).
* Corresponding author.

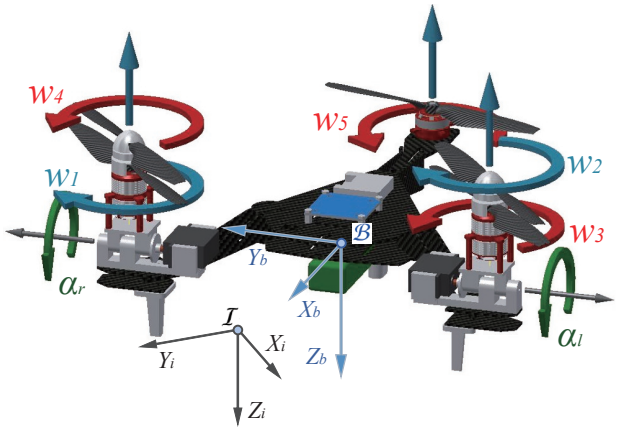

Fig. 1. Schematic of the CTRUAV with the body-fixed frame and inertial frame.

bus A400M [17], Kamov series helicopter [18], single-axis coaxial-rotor UAV [19], and six-axis coaxial tilt-rotor UAV [20]. Comparing to the single-rotor scheme, the coaxial-rotor scheme has smaller rotor diameter and rotational inertia. Hence the corresponding speed of the rotate velocity of the coaxial rotors is faster, the overall dimension of the CTRUAV is smaller, and the CTRUAV can take off and land in a smaller ground and fly in a narrower space. In addition, the Coriolis force and the reaction torques, and the unbalanced torques caused by airspeed difference on blades of the rotors are counteracted by its structural symmetry. Comparing to the six-axis coaxial tilt-rotor UAV proposed in [20], which includes six pairs of tiltable coaxial rotors and can realize omnidirectional flight, the structure of the proposed CTRUAV is simpler, and follows simpler control strategy.

Despite the advantages of the CTRUAV mentioned above, due to the underactuated property, it is challenging to design an effective controller for the CTRUAV. In this paper, the following problems are discussed. Firstly, the CTRUAV is an underactuated system, its lateral maneuver can only be realized by rolling the CTRUAV to the desired direction. The proposed controller is designed in cascade form to overcome the underactuated property of the CTRUAV, so that the CTRUAV can track desired pitch angle, yaw angle, and velocities in three directions, and stabilize the roll angle. Furthermore, the CTRUAV's strong nonlinearity and coupled dynamics will increase the complexity of control design, so we design feedforward compensation for these dynamics. At last, since the control allocation of CTRUAV is different from other TRUAVs, the distributive law is newly designed according to the special configuration of the CTRUAV. To evaluate the performance of the proposed controller, simulations are firstly carried out in Matlab/SimMechanics environment [21], and then real flight tests are performed to further validate the effectiveness of the designed controller outdoors.

The main contributions of this work are summarized as follows. Firstly, a nonlinear cascade controller is proposed using backstepping-like feedback linearization to track outputs specified by the attitude and velocity of the CTRUAV, and the special Lyapunov candidate functions are designed to analyze the stability of the resulting closed-loop system. Secondly, the control allocation is newly designed according to the special mechanism of the CTRUAV.

The remainder of this paper is organized as follows: In Section 2, the structure of the CTRUAV is introduced, and its dynamical model is presented. A nonlinear controller with a cascade structure is detailed in Section 3. In Section 4, the performance of the designed closed-loop control system is evaluated in simulations, and its effectiveness is further validated in real flight tests outdoors. At last, conclusions are presented in Section 5.

2. THE STRUCTURE AND THE DYNAMIC MODEL OF THE CTRUAV

In this section, the structure of the CTRUAV is introduced, and its dynamic model is presented. The air drag force which influences the dynamic of the CTRUAV is taken into consideration in the dynamic model.

The general structure of the CTRUAV is illustrated in Fig. 2, which consists of a carbon-fiber fuselage, two tiltable coaxial-rotor modules, a rear rotor module, a flight control system, a power source, and a distribution plate. The carbon-fiber fuselage includes a main plate and three arms. On the main plate, the flight control system, the power system, and the distribution plate are installed. The tiltable coaxial-rotor module consists of two coaxial 2208 DC motors, two 8040 rotors, two 20-Amp electronic speed controllers (ESCs), a 3D printing tilt motor base, and a servo. The response speed of the chosen ESCs and servos is fast, and their response time is neglected in this work. The electronic flight control system utilizes an STM32F405 microprogrammed control unit (MCU) with a maximum working frequency of 168MHz to process the designed control algorithm, an inertial measurement unit

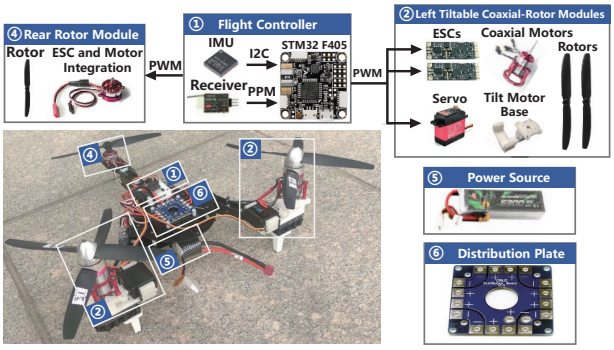

Fig. 2. The general configuration of the CTRUAV.

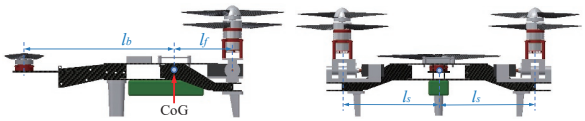

(a) Side view. (b) Front view.

Fig. 3. The geometric distances of the CTRUAV.

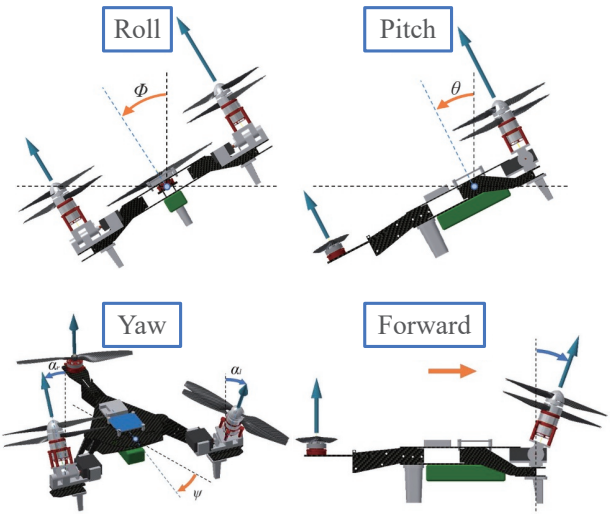

Fig. 4. The mechanisms of the CTRUAV's maneuvers.

(IMU) integrated an accelerometer and a gyroscope, and a control signal receiver. The flight control system processes the control algorithm and outputs pulse width modification (PWM) signals to servos to control the tilt angles and ESCs to control the thrusts of the rotors. The IMU measures the velocity and the attitude of the CTRUAV and communicates with MCU by I2C bus at the frequency of 100Hz.

The key geometric distances of the CTRUAV are depicted in Fig. 3. The overall mechanisms of the CTRUAV are demonstrated in Fig. 4. The physical parameters of the CTRUAV, such as mass, rotational inertia, and thrust coefficients, are set in accordance with the real CTRUAV and listed in Table 1. The coefficients of c_{tf}, c_t, and c_q are measured by the methods proposed in the previous work in [22].

To construct the dynamic model of the CTRUAV, the reference frames are firstly defined as follows. As shown in Fig. 1, the inertial frame $\mathscr{I}\{X_i, Y_i, Z_i\}$ follows the North-East-Down (NED) notation, and the body-fixed frame $\mathscr{B}\{X_b, Y_b, Z_b\}$, whose origin coincides with the center of gravity (CoG) of the CTRUAV, follows the standard aircraft notation where the X_b, Y_b, and Z_b points the longitudinal flight direction, the right direction, and downward direction, respectively.

Based on the two reference frames described above, the variables are defined as follows:

Table 1. Physical parameters.

Parameter	Description	Value	Unit
g	Gravity	9.807	m/s^2
m_q	Mass of CTRUAV	0.979	kg
l_f	Distance	0.078	m
l_b	Distance	0.24	m
l_s	Distance	0.151	m
I_x	Roll inertia of CTRUAV	4.11×10^{-3}	kg·m^2
I_y	Pitch inertia of CTRUAV	6.3×10^{-3}	kg·m^2
I_z	Yaw inertia of CTRUAV	9.85×10^{-3}	kg·m^2
c_{tf}	Lift coefficient of coaxial rotors	1.63×10^{-5}	N/(rad/s)^2
c_t	Lift coefficient of rear rotor	9.6×10^{-6}	N/(rad/s)^2
c_q	Torque coefficient of rear rotor	2.4×10^{-7}	N/(rad/s)^2

- $\boldsymbol{q} = [\boldsymbol{\xi}^\top \ \boldsymbol{\eta}^\top]^\top \in \mathbb{R}^6$ - generalized coordinates;
- $\boldsymbol{\xi} = [x \ y \ z]^\top \in \mathbb{R}^3$ - position of the origin of $\mathscr{B}$ measured in inertial frame $\mathscr{I}$, where x, y, and z are positions along X_i, Y_i, and Z_i, respectively;
- $\boldsymbol{\eta} = [\phi \ \theta \ \psi]^\top \in \mathbb{R}^3$ - attitude angle of CTRUAV in Euler coordinate system with the roll angle ϕ, the pitch angle θ, and the yaw angle ψ, and they are limited as

$$\phi, \ \theta \in (-\pi/2, \ \pi/2), \ \psi \in (-\pi, \ \pi); \tag{1}$$

- $\boldsymbol{\Omega} = [\omega_x \ \omega_y \ \omega_z]^\top$ - angular velocity of $\mathscr{B}$ relative to $\mathscr{I}$ expressed in $\mathscr{B}$;
- $\dot{\boldsymbol{\xi}}_{\boldsymbol{b}} = [\dot{x}_b \ \dot{y}_b \ \dot{z}_b]^\top \in \mathbb{R}^3$ - linear velocity of the origin of $\mathscr{B}$ relative to $\mathscr{I}$ expressed in inertial frame $\mathscr{B}$, where $\dot{x}_b$, $\dot{y}_b$, and $\dot{z}_b$ are velocity along X_b, Y_b, and Z_b, respectively.

The relationship between the velocity vectors $\dot{\boldsymbol{\xi}}_{\boldsymbol{b}}$,$\boldsymbol{\Omega}$ and $\dot{\boldsymbol{\xi}}$, $\dot{\boldsymbol{\eta}}$ are given as

$$\dot{\boldsymbol{\xi}} = \boldsymbol{R}_{\boldsymbol{t}} \dot{\boldsymbol{\xi}}_{\boldsymbol{b}}, \boldsymbol{\Omega} = \boldsymbol{R}_{\boldsymbol{r}} \dot{\boldsymbol{\eta}}, \tag{2}$$

where $\boldsymbol{R}_{\boldsymbol{t}}$ is the transformation matrix between the body frame $\mathscr{B}$ and the inertial frame $\mathscr{I}$ [23], and is expressed as

$$\boldsymbol{R}_{\boldsymbol{t}} = \begin{bmatrix} \boldsymbol{c\theta c\psi} & \boldsymbol{s\phi s\theta c\psi - c\phi s\psi} & \boldsymbol{c\phi s\theta c\psi + s\phi s\psi} \\ \boldsymbol{c\theta s\psi} & \boldsymbol{s\phi s\theta s\psi + c\phi c\psi} & \boldsymbol{c\phi s\theta s\psi - s\phi c\psi} \\ \boldsymbol{-s\theta} & \boldsymbol{s\phi c\theta} & \boldsymbol{c\phi c\theta} \end{bmatrix},$$

and $\boldsymbol{R}_{\boldsymbol{r}} = \begin{bmatrix} 1 & 0 & \boldsymbol{-s\theta} \\ 0 & \boldsymbol{c\phi} & \boldsymbol{s\phi c\theta} \\ 0 & \boldsymbol{-s\phi} & \boldsymbol{c\phi c\theta} \end{bmatrix}$ is the rotation velocity matrix [23].

Throught this paper, $\boldsymbol{s}$ and $\boldsymbol{c}$ represent for *sin* and *cos*, $\boldsymbol{0}_{m\times n}$ stands for $m \times n$ dimensional null matrix, and $\boldsymbol{I}_n$ stands for n-dimensional identity matrix, respectively.

In this work, the CTRUAV is simplified as a rigid body with six degrees of freedom. The dynamic model of the

CTRUAV is presented based on the work of [24] as follows:

$$\boldsymbol{R_t}\left(\boldsymbol{F}+\boldsymbol{D_{\xi b}}\right)+m\boldsymbol{g}=m\ddot{\boldsymbol{\xi}}, \tag{3a}$$

$$\boldsymbol{\tau}+\boldsymbol{D_\Omega}-\boldsymbol{\Omega}\times(\boldsymbol{I\Omega})=\boldsymbol{I}[\boldsymbol{R_r}\ddot{\boldsymbol{\eta}}+(\frac{\partial \boldsymbol{R_r}}{\partial\phi}\dot{\phi}+\frac{\partial \boldsymbol{R_r}}{\partial\theta}\dot{\theta})\dot{\boldsymbol{\eta}}]. \tag{3b}$$

where $\boldsymbol{g}=[0\ 0\ g]^\top$, with the acceleration due to gravity g, m is the mass of the CTRUAV, $\boldsymbol{I}=\mathrm{diag}(I_x\ I_y\ I_z)$ is the rotational inertia matrix of the CTRUAV.

The details of system (3) are elaborated as follows. The force $\boldsymbol{F}=[F_{xb}\ 0\ F_{zb}]^\top$ in (3a) and torque $\boldsymbol{\tau}=[\tau_{xb}\ \tau_{yb}\ \tau_{zb}]^\top$ in (3b) are produced by the rotors of the CTRUAV, which are given by

$$\begin{bmatrix}F_{xb}\\F_{zb}\\\tau_\phi\\\tau_\theta\\\tau_\psi\end{bmatrix}=\begin{bmatrix}F_r\boldsymbol{s}\alpha_r+F_l\boldsymbol{s}\alpha_l\\-F_r\boldsymbol{c}\alpha_r-F_l\boldsymbol{c}\alpha_l-F_b\\(-F_r\boldsymbol{c}\alpha_r+F_l\boldsymbol{c}\alpha_l)l_s+\tau_r\boldsymbol{s}\alpha_r+\tau_l\boldsymbol{s}\alpha_l\\F_r\boldsymbol{c}\alpha_r l_f+F_l\boldsymbol{c}\alpha_l l_f-F_b l_b\\-F_r\boldsymbol{s}\alpha_r l_s+F_l\boldsymbol{s}\alpha_l l_s+\tau_b-\tau_r\boldsymbol{c}\alpha_r-\tau_l\boldsymbol{c}\alpha_r\end{bmatrix}, \tag{4}$$

where α_r and α_l are the tilt angles of the right and left coaxial-rotor modules, respectively, F_r, F_l, and F_b are the thrusts produced by right coaxial rotors, left coaxial rotors, and rear rotor, respectively, τ_r, τ_l, and τ_b are the reaction torques produced by the right coaxial rotors, the left coaxial rotors, and the rear rotor, respectively. The forces F_r, F_l, F_b and the reaction torques τ_r, τ_l, τ_b are given by

$$F_r=c_{tf}(\omega_1^2+\omega_4^2), F_l=c_{tf}(\omega_2^2+\omega_3^2), F_b=c_t\omega_5^2,$$
$$\tau_r=c_{qf}(-\omega_1^2+\omega_4^2), \tau_l=c_{qf}(-\omega_2^2+\omega_3^2), \tau_b=c_q\omega_5^2$$

with the rotational speed ω_i of rotor $i(i=1\sim5)$ illustrated in Fig. 1, the thrust coefficients c_{tf}, c_t, and the torque coefficients c_{qf}, c_q. The rotational velocities of each pair of coaxial rotors are set to the opposite to counteract the reaction torque on the coaxial rotors, which means the coaxial rotors produce no reaction torque, and $\omega_1=\omega_4=\omega_r$, $\omega_2=\omega_3=\omega_l$. Then, (4) is rewritten as

$$\begin{bmatrix}F_{xb}\\F_{zb}\\\tau_\phi\\\tau_\theta\\\tau_\psi\end{bmatrix}=\begin{bmatrix}2c_{tf}&0&2c_{tf}&0&0\\0&-2c_{tf}&0&-2c_{tf}&-c_t\\0&-2c_{tf}l_s&0&2c_{tf}l_s&0\\0&2c_{tf}l_f&0&2c_{tf}l_f&-c_t l_b\\-2c_{tf}l_s&0&2c_{tf}l_s&0&c_q\end{bmatrix}\times\begin{bmatrix}\boldsymbol{s}\alpha_r\omega_r^2\\\boldsymbol{c}\alpha_r\omega_r^2\\\boldsymbol{s}\alpha_l\omega_l^2\\\boldsymbol{c}\alpha_l\omega_l^2\\\omega_5^2\end{bmatrix}. \tag{5}$$

The air drag force $\boldsymbol{D_{\xi b}}$ in (3a) and the drag troque $\boldsymbol{D_\Omega}$ in (3b) on the CTRUAV are introduced, where $\boldsymbol{D_{\xi b}}=-[D_{xb}\dot{x}_b|\dot{x}_b|\ \ D_{yb}\dot{y}_b|\dot{y}_b|\ \ D_{zb}\dot{z}_b|\dot{z}_b|]^\top$, $\boldsymbol{D_\Omega}=-[D_{wx}\omega_x|\omega_x|\ \ D_{wy}\omega_y|\omega_y|\ \ D_{wz}\omega_z|\omega_z|]^\top$ with the drag torque force coefficients D_{xb}, D_{yb}, and D_{zb} which are obtained by the methods proposed in the previous work [22], and the drag torque torque coefficients D_{wx}, D_{wy}, and D_{wz}.

Then, for ease-of-use, the dynamic model (3) is rewritten as

$$\ddot{\boldsymbol{\xi}}=\boldsymbol{F_\xi}/m+\boldsymbol{h_\xi}, \tag{6a}$$
$$\ddot{\boldsymbol{\eta}}=\boldsymbol{g_\eta}\boldsymbol{\tau}+\boldsymbol{h_\eta}, \tag{6b}$$

where

$$\boldsymbol{F_\xi}=\boldsymbol{R_t}\boldsymbol{F},$$
$$\boldsymbol{h_\xi}=\boldsymbol{R_t}\boldsymbol{D_{\xi b}}/m+\boldsymbol{g},$$
$$\boldsymbol{g_\eta}=\boldsymbol{R_r}^{-1}\boldsymbol{I}^{-1}(\boldsymbol{R_r}^\top)^{-1},$$
$$\boldsymbol{h_\eta}=\boldsymbol{R_r}^{-1}\boldsymbol{I}^{-1}\Bigg(\boldsymbol{D_\Omega}-\boldsymbol{R_r}\dot{\boldsymbol{\eta}}\times(\boldsymbol{IR_r}\dot{\boldsymbol{\eta}})-\boldsymbol{I}\left(\frac{\partial \boldsymbol{R_r}}{\partial\phi}\dot{\phi}+\frac{\partial \boldsymbol{R_r}}{\partial\theta}\dot{\theta}\right)\dot{\boldsymbol{\eta}}\Bigg).$$

Remark 1: In this work, the deadzones of the servos are not taken into consideration in control design for the CTRUAV, and assume that the response speed of the servos is fast and the tilt angles α_r and α_l can always track the desired values. To solve the problem caused by actuator deadzones, the adaptive Fuzzy control method proposed in [25] can be applied.

3. CONTROL DESIGN AND STABILITY ANALYSIS

The main object of this section is to design a control strategy to track the desired attitude $\boldsymbol{\eta_d}$ and velocity $\dot{\boldsymbol{\xi}}_{\boldsymbol{d}}$. The CTRUAV has six degrees of freedom (DoFs) with only five control inputs F_{xb}, F_{zb}, τ_ϕ, τ_θ, and τ_ψ, which is known as the underactuated property [22]. The control strategy is designed in a cascade structure to overcome this property. The proposed controller includes an outer-loop velocity controller and an inner-loop attitude controller. The structure of the control strategy is described in Fig. 5.

The tracking errors for the velocity $\dot{\boldsymbol{\xi}}$ and attitude $\boldsymbol{\eta}$ will be defined for the following controller design and stability analysis.

Considering the attitude error and angular velocity error of the CTRUAV, the attitude error and the angular velocity error of the CTRUAV are defined as

$$\boldsymbol{e_\eta}\triangleq\boldsymbol{\eta}_d-\boldsymbol{\eta}, \boldsymbol{e_{\dot\eta}}\triangleq\dot{\boldsymbol{\eta}}_d-\dot{\boldsymbol{\eta}}, \tag{7}$$

where $\boldsymbol{e_\eta}=[e_\phi\ e_\theta\ e_\psi]^\top$, $\boldsymbol{e_{\dot\eta}}=[e_{\dot\phi}\ e_{\dot\theta}\ e_{\dot\psi}]^\top$, and $\boldsymbol{\eta}_d$ is the desired attitude of the CTRUAV, $\dot{\boldsymbol{\eta}}_d$ is the desired Euler angular velocity and equal to zero.

Considering the velocity error of the CTRUAV, the velocity error of the CTRUAV is defined as

$$\boldsymbol{e_{\dot\xi}}\triangleq\dot{\boldsymbol{\xi}}_d-\dot{\boldsymbol{\xi}}, \tag{8}$$

where $\boldsymbol{e}_{\dot{\boldsymbol{\xi}}} = [e_{\dot{x}}\ e_{\dot{y}}\ e_{\dot{z}}]^\top$ and $\dot{\boldsymbol{\xi}}_d$ is the constant desired velocity of the CTRUAV.

3.1. Inner-loop attitude controller

For (3b), the inner-loop controller is applied to control the attitude $\boldsymbol{\eta}$ of the CTRUAV. We define

$$\boldsymbol{e}_{\dot{\boldsymbol{\eta}},\boldsymbol{\eta}} = \boldsymbol{e}_{\dot{\boldsymbol{\eta}}} + \boldsymbol{a}_{\boldsymbol{\eta}}\boldsymbol{e}_{\boldsymbol{\eta}}, \tag{9}$$

where $\boldsymbol{a}_{\boldsymbol{\eta}} = \mathrm{diag}(a_\phi, a_\theta, a_\psi)$ is a positive definite diagonal matrix. The torque $\boldsymbol{\tau}$ is designed as

$$\boldsymbol{\tau} = \boldsymbol{g}_{\boldsymbol{\eta}}^{-1}\left(\boldsymbol{b}_{\boldsymbol{\eta}}\boldsymbol{e}_{\dot{\boldsymbol{\eta}},\boldsymbol{\eta}} - \boldsymbol{h}_{\boldsymbol{\eta}} + \boldsymbol{a}_{\boldsymbol{\eta}}\boldsymbol{e}_{\dot{\boldsymbol{\eta}}}\right), \tag{10}$$

where $\boldsymbol{b}_{\boldsymbol{\eta}} = \mathrm{diag}(b_\phi, b_\theta, b_\psi)$ is also positive definite.

Theorem 1: Consider the subsystem described in (3b), the desired Euler angle $\boldsymbol{\eta}_d$ is a constant and $\dot{\boldsymbol{\eta}}_d = 0$. If the control torque $\boldsymbol{\tau}_{\boldsymbol{\eta}}$ in (10) is applied, the zero equilibria of the errors $\boldsymbol{e}_{\boldsymbol{\eta}}$ and $\boldsymbol{e}_{\dot{\boldsymbol{\eta}}}$ are asymptotically stable.

Proof: The Lyapunov candidate $V_{\boldsymbol{\eta}}$ is defined as

$$V_{\boldsymbol{\eta}}(\boldsymbol{e}_{\dot{\boldsymbol{\eta}},\boldsymbol{\eta}}) = \|\boldsymbol{e}_{\dot{\boldsymbol{\eta}},\boldsymbol{\eta}}\|^2/2. \tag{11}$$

Since $\dot{\boldsymbol{\eta}}_d = 0$, its derivative $\ddot{\boldsymbol{\eta}}_d = 0$, and the derivate of $\boldsymbol{e}_{\dot{\boldsymbol{\eta}},\boldsymbol{\eta}}$ in (9) with respect to time is

$$\dot{\boldsymbol{e}}_{\dot{\boldsymbol{\eta}},\boldsymbol{\eta}} = -\ddot{\boldsymbol{\eta}} + \boldsymbol{a}_{\boldsymbol{\eta}}\boldsymbol{e}_{\dot{\boldsymbol{\eta}}}.$$

Substituting (6b) into above equation, we have

$$\dot{\boldsymbol{e}}_{\dot{\boldsymbol{\eta}},\boldsymbol{\eta}} = -\boldsymbol{g}_{\boldsymbol{\eta}}\boldsymbol{\tau} - \boldsymbol{h}_{\boldsymbol{\eta}} + \boldsymbol{a}_{\boldsymbol{\eta}}\boldsymbol{e}_{\dot{\boldsymbol{\eta}}}.$$

Substituting (10) into above equation, the time derivative $\dot{\boldsymbol{s}}$ is derived as

$$\dot{\boldsymbol{e}}_{\dot{\boldsymbol{\eta}},\boldsymbol{\eta}} = -\boldsymbol{b}_{\boldsymbol{\eta}}\boldsymbol{e}_{\dot{\boldsymbol{\eta}},\boldsymbol{\eta}}. \tag{12}$$

Then, the time derivative of the Lyapunov candidate (11) is derived as

$$\dot{V}_{\boldsymbol{\eta}} = \boldsymbol{e}_{\dot{\boldsymbol{\eta}},\boldsymbol{\eta}}{}^\top\dot{\boldsymbol{e}}_{\dot{\boldsymbol{\eta}},\boldsymbol{\eta}} = -\boldsymbol{e}_{\dot{\boldsymbol{\eta}},\boldsymbol{\eta}}{}^\top\boldsymbol{b}_{\boldsymbol{\eta}}\boldsymbol{e}_{\dot{\boldsymbol{\eta}},\boldsymbol{\eta}} = -\lambda_\eta V_{\boldsymbol{\eta}}, \tag{13}$$

where $\lambda_\eta = 2\min(b_\phi, b_\theta, b_\psi)$ is a positive constant.

Hence, the zero equilibrium of $V_{\boldsymbol{\eta}}$ is exponentially stable. When $V_{\boldsymbol{\eta}} = 0$, we have $\boldsymbol{e}_{\dot{\boldsymbol{\eta}},\boldsymbol{\eta}} = \boldsymbol{0}$, and $\dot{\boldsymbol{e}}_{\boldsymbol{\eta}} = -\boldsymbol{a}_{\boldsymbol{\eta}}\boldsymbol{e}_{\boldsymbol{\eta}}$, the zero equilibrium of the attitude error $\boldsymbol{e}_{\boldsymbol{\eta}}$ is exponentially stable. Consequently, it can be concluded that zero equilibrium of the attitude error $\boldsymbol{e}_{\boldsymbol{\eta}}$ is locally asymptotically stable. □

3.2. Outer-loop velocity controller

The outer-loop velocity controller, as illustrated in Fig. 5, is applied to control the velocity $\dot{\boldsymbol{\xi}}$ of the CTRUAV.

The desired force $\boldsymbol{F}_{\boldsymbol{\xi d}}$ of $\boldsymbol{F}_{\boldsymbol{\xi}}$ in (6a) is designed as

$$\boldsymbol{F}_{\boldsymbol{\xi d}} = [F_{xd}\ F_{yd}\ F_{zd}]^\top = m\boldsymbol{K}_{\dot{\boldsymbol{\xi}}}\boldsymbol{e}_{\dot{\boldsymbol{\xi}}} - m\boldsymbol{h}_{\boldsymbol{\xi}}, \tag{14}$$

where $\boldsymbol{K}_{\dot{\boldsymbol{\xi}}} = \mathrm{diag}(k_{\dot{x}}, k_{\dot{y}}, k_{\dot{z}})$ is positive definite.

Theorem 2: For the dynamical model of the CTRUAV defined in (6a), with a fixed desired reference velocity $\dot{\boldsymbol{\xi}}_d$, if the resultant force $\boldsymbol{F}_\xi$ is set as $\boldsymbol{F}_{\boldsymbol{\xi d}}$ in (14), the zero equilibrium of the velocity tracking error $\boldsymbol{e}_{\dot{\boldsymbol{\xi}}}$ is exponentially stable.

Proof: The time derivative of the velocity error $\boldsymbol{e}_{\dot{\boldsymbol{\xi}}}$ of the CTRUAV is $\dot{\boldsymbol{e}}_{\dot{\boldsymbol{\xi}}} = \ddot{\boldsymbol{\xi}}_d - \ddot{\boldsymbol{\xi}}$. Considering $\dot{\boldsymbol{\xi}}_d$ is constant, we have $\ddot{\boldsymbol{\xi}}_d = 0$. Then, substituting dynamic model (6a) into $\dot{\boldsymbol{e}}_{\dot{\boldsymbol{\xi}}} = -\ddot{\boldsymbol{\xi}}$, we have

$$\dot{\boldsymbol{e}}_{\dot{\boldsymbol{\xi}}} = -\boldsymbol{F}_{\boldsymbol{\xi}}/m - \boldsymbol{h}_{\boldsymbol{\xi}}. \tag{15}$$

Define

$$\boldsymbol{e}_{F\xi} \triangleq \boldsymbol{F}_{\boldsymbol{\xi d}} - \boldsymbol{F}_{\boldsymbol{\xi}}, \tag{16}$$

where $\boldsymbol{F}_{\boldsymbol{\xi d}}$ is given in (14). Substituting control input error (16) and (14) into (15) yields

$$\dot{\boldsymbol{e}}_{\dot{\boldsymbol{\xi}}}(\boldsymbol{e}_{\dot{\boldsymbol{\xi}}}, \boldsymbol{e}_{F\xi}) = -\boldsymbol{K}_{\dot{\boldsymbol{\xi}}}\boldsymbol{e}_{\dot{\boldsymbol{\xi}}} + \boldsymbol{e}_{F\xi}/m. \tag{17}$$

Setting $\boldsymbol{F}_{\boldsymbol{\xi}}$ as $\boldsymbol{F}_{\boldsymbol{\xi d}}$, which means $\boldsymbol{e}_{F\xi} = 0$, we can get

$$\dot{\boldsymbol{e}}_{\dot{\boldsymbol{\xi}}}(\boldsymbol{e}_{\dot{\boldsymbol{\xi}}}, 0) = -\boldsymbol{K}_{\dot{\boldsymbol{\xi}}}\boldsymbol{e}_{\dot{\boldsymbol{\xi}}}. \tag{18}$$

The Lyapunov candidate $V_{\dot{\boldsymbol{\xi}}}$ is defined to check the validity of the outer-loop velocity controller,

$$V_{\dot{\boldsymbol{\xi}}}(\boldsymbol{e}_{\dot{\boldsymbol{\xi}}}) = \|\boldsymbol{e}_{\dot{\boldsymbol{\xi}}}\|^2/2. \tag{19}$$

Substituting (18) into the derivative of (19), we have $\dot{V}_{\dot{\boldsymbol{\xi}}} = (\partial V_{\dot{\boldsymbol{\xi}}}/\partial \boldsymbol{e}_{\dot{\boldsymbol{\xi}}})\dot{\boldsymbol{e}}_{\dot{\boldsymbol{\xi}}}(\boldsymbol{e}_{\dot{\boldsymbol{\xi}}}, 0) = -\boldsymbol{e}_{\dot{\boldsymbol{\xi}}}^\top\boldsymbol{K}_{\dot{\boldsymbol{\xi}}}\boldsymbol{e}_{\dot{\boldsymbol{\xi}}}$. According to the previous content, $\boldsymbol{K}_{\dot{\boldsymbol{\xi}}}$ is positive definite. Hence,

$$\dot{V}_{\dot{\boldsymbol{\xi}}} = \frac{\partial V_{\dot{\boldsymbol{\xi}}}}{\partial \boldsymbol{e}_{\dot{\boldsymbol{\xi}}}}\dot{\boldsymbol{e}}_{\dot{\boldsymbol{\xi}}}(\boldsymbol{e}_{\dot{\boldsymbol{\xi}}}, 0) \le -\lambda_{\dot{\boldsymbol{\xi}}}\|\boldsymbol{e}_{\dot{\boldsymbol{\xi}}}\|^2, \tag{20}$$

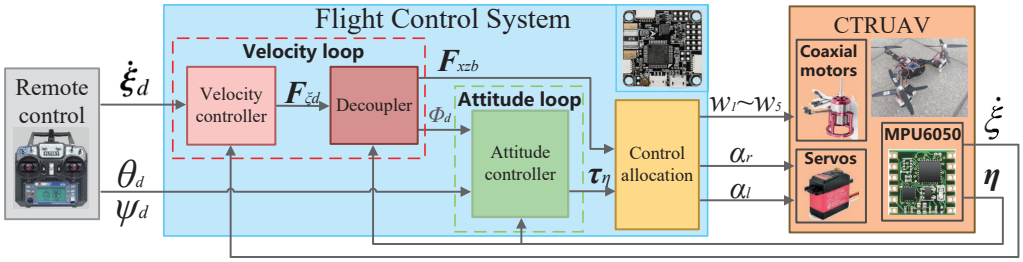

Fig. 5. The schematic of the controller of the CTRUAV system.

where $\lambda_{\dot{\xi}} = \lambda_{min}(\boldsymbol{K}_{\dot{\xi}})$, $\lambda_{min}(\cdot)$ denotes the minimum eigenvalue of a matrix. Therefore, if $\boldsymbol{F_\xi} = \boldsymbol{F_{\xi d}}$, the zero equilibrium of the velocity tracking errors $\boldsymbol{e_{\dot{\xi}}}$ of the CTRUAV are locally exponentially stable. □

Next, the desired roll angle ϕ_d and the rotors' thrust forces $\boldsymbol{F} = [F_{xb}\ 0\ F_{zb}]^\top$ will be obtained by transforming from the desired resultant force $\boldsymbol{F_{\xi d}}$ in (14). Noting $\boldsymbol{F_\xi} = \boldsymbol{R_t F}$ in (6a), the relationship between $\boldsymbol{F}$, ϕ_d, and $\boldsymbol{F_{\xi d}}$ satisfies

$$\boldsymbol{F_{\xi d}} = \boldsymbol{R}_d \boldsymbol{F}, \tag{21}$$

where $\boldsymbol{R}_d = \begin{bmatrix} \boldsymbol{c}\psi & -\boldsymbol{s}\psi & 0 \\ \boldsymbol{s}\psi & \boldsymbol{c}\psi & 0 \\ 0 & 0 & 1 \end{bmatrix} \begin{bmatrix} \boldsymbol{c}\theta & 0 & \boldsymbol{s}\theta \\ 0 & 1 & 0 \\ -\boldsymbol{s}\theta & 0 & \boldsymbol{c}\theta \end{bmatrix} \begin{bmatrix} 1 & 0 & 0 \\ 0 & \boldsymbol{c}\phi_d & -\boldsymbol{s}\phi_d \\ 0 & \boldsymbol{s}\phi_d & \boldsymbol{c}\phi_d \end{bmatrix}$.
Then, F_{xb}, F_{zb}, and ϕ_d is obtained as

$$\phi_d = \arctan\left(\frac{F_{xd}\boldsymbol{s}(\psi) - F_{yd}\boldsymbol{c}(\psi)}{F_{xd}\boldsymbol{s}(\theta)\boldsymbol{c}(\psi) + F_{yd}\boldsymbol{s}(\theta)\boldsymbol{s}(\psi) + F_{zd}\boldsymbol{c}(\theta)}\right), \tag{22a}$$

$$F_{xb} = F_{xd}\boldsymbol{c}(\theta)\boldsymbol{c}(\psi) + F_{yd}\boldsymbol{c}(\theta)\boldsymbol{s}(\psi) - F_{zd}\boldsymbol{s}(\theta), \tag{22b}$$

$$F_{zb} = \frac{F_{xd}\boldsymbol{s}(\theta)\boldsymbol{c}(\psi) + F_{yd}\boldsymbol{s}(\theta)\boldsymbol{s}(\psi) + F_{zd}\boldsymbol{c}(\theta)}{\boldsymbol{c}\phi_d}. \tag{22c}$$

Considering the constrains in (1) and the mechanisms of the CTRUAV, we have $F_{zb} \geq 0$ and $F_{xd}\boldsymbol{s}(\theta)\boldsymbol{c}(\psi) + F_{yd}\boldsymbol{s}(\theta)\boldsymbol{s}(\psi) + F_{zd}\boldsymbol{c}(\theta) \geq 0$ in (22c). In (22a), if $F_{xd}\boldsymbol{s}(\theta)\boldsymbol{c}(\psi) + F_{yd}\boldsymbol{s}(\theta)\boldsymbol{s}(\psi) + F_{zd}\boldsymbol{c}(\theta) = 0$, we set ϕ_d as follows to avoid the singularity problem

$$\phi_d = \begin{cases} b_\phi, & F_{xd}\boldsymbol{s}(\psi) - F_{yd}\boldsymbol{c}(\psi) > 0, \\ -b_\phi, & F_{xd}\boldsymbol{s}(\psi) - F_{yd}\boldsymbol{c}(\psi) < 0, \\ \phi, & F_{xd}\boldsymbol{s}(\psi) - F_{yd}\boldsymbol{c}(\psi) = 0, \end{cases}$$

where b_ϕ is a given positive value less than $\pi/2$.

3.3. Stability analysis of the close-loop system

The stability of the inner-loop system and the outer-loop system has been proved in the subsections. However, the stability of the whole resulting closed-loop CTRUAV system need to be further examined.

Theorem 3: For the dynamical model of the CTRUAV in (6), with a fixed desired reference velocity $\dot{\boldsymbol{\xi}}_d$. If the designed controllers (10) and (14) are applied to control the CTRUAV, the zero equilibria of the errors $\boldsymbol{e_{\dot{\xi}}}$ and $\boldsymbol{e_\eta}$ are asymptotically stable.

Proof: The Lyapunov candidate $V_t(\boldsymbol{e_{\dot{\xi}}}, \boldsymbol{s})$ is constructed to analyze the stability of the CTRUAV system as follows:

$$V_t(\boldsymbol{e_{\dot{\xi}}}, \boldsymbol{e_{\dot{\eta},\eta}}) = k_1 V_{\dot{\xi}}(\boldsymbol{e_{\dot{\xi}}}) + k_2\|\boldsymbol{e_\eta}\|^2 + \|\boldsymbol{e_{\dot{\eta},\eta}}\|^2, \tag{23}$$

where $\boldsymbol{k_\eta} = \mathrm{diag}(k_\phi, k_\theta, k_\psi)$ is positive definite, with

$$k_\chi = \left(a_\chi + b_\chi + \sqrt{(a_\chi + b_\chi)^2 + 4a_\chi b_\chi - k_2}\right)/2, \tag{24}$$

for $\chi \in \{\phi, \theta, \psi\}$, and

$$k_1 < 2\lambda_{\boldsymbol{\eta}}^{'}\lambda_{\dot{\boldsymbol{\xi}}}/L^2,$$
$$k_2 \leq \min_{\chi\in\{\phi,\theta,\psi\}}\left((a_\chi + b_\chi)^2 + 4a_\chi b_\chi\right), \tag{25}$$

with $\lambda_{\dot{\boldsymbol{\xi}}}$, L and $\lambda_{\boldsymbol{\eta}}^{'}$ defined in equations (20), (27), and (28), respectively. The time derivative $\dot{V}_t$ of V_t in (23) is deduced as

$$\dot{V}_t = k_1\frac{\partial V_{\dot{\xi}}}{\partial \boldsymbol{e_{\dot{\xi}}}}\dot{\boldsymbol{e}}_{\dot{\xi}}(\boldsymbol{e_{\dot{\xi}}}, \boldsymbol{e_{F\xi}}) + k_2\boldsymbol{e_\eta}^\top\boldsymbol{e_{\dot{\eta}}} + (\boldsymbol{e_{\dot{\eta}}} + \boldsymbol{k_\eta}\boldsymbol{e_\eta})^\top(\boldsymbol{k_\eta}\boldsymbol{e_{\dot{\eta}}} - \ddot{\boldsymbol{\eta}}).$$

Substituting (6b) and (10) into above equation, we have

$$\begin{aligned}\dot{V}_t &= k_1\frac{\partial V_{\dot{\xi}}}{\partial \boldsymbol{e_{\dot{\xi}}}}\dot{\boldsymbol{e}}_{\dot{\xi}}(\boldsymbol{e_{\dot{\xi}}}, 0) \\ &\quad + k_1\frac{\partial V_{\dot{\xi}}}{\partial \boldsymbol{e_{\dot{\xi}}}}[\dot{\boldsymbol{e}}_{\dot{\xi}}(\boldsymbol{e_{\dot{\xi}}}, \boldsymbol{e_{F\xi}}) - \dot{\boldsymbol{e}}_{\dot{\xi}}(\boldsymbol{e_{\dot{\xi}}}, 0)] + k_2\boldsymbol{e_\eta}^\top\boldsymbol{e_{\dot{\eta}}} \\ &\quad + (\boldsymbol{e_{\dot{\eta}}} + \boldsymbol{k_\eta}\boldsymbol{e_\eta})^\top((\boldsymbol{k_\eta} - \boldsymbol{a_\eta} - \boldsymbol{b_\eta})\boldsymbol{e_{\dot{\eta}}} - \boldsymbol{a_\eta}\boldsymbol{b_\eta}\boldsymbol{e_\eta}) \\ &= k_1\frac{\partial V_{\dot{\xi}}}{\partial \boldsymbol{e_{\dot{\xi}}}}\dot{\boldsymbol{e}}_{\dot{\xi}}(\boldsymbol{e_{\dot{\xi}}}, 0) \\ &\quad + k_1\frac{\partial V_{\dot{\xi}}}{\partial \boldsymbol{e_{\dot{\xi}}}}[\dot{\boldsymbol{e}}_{\dot{\xi}}(\boldsymbol{e_{\dot{\xi}}}, \boldsymbol{e_{F\xi}}) - \dot{\boldsymbol{e}}_{\dot{\xi}}(\boldsymbol{e_{\dot{\xi}}}, 0)] \\ &\quad - \boldsymbol{e_\eta}^\top\boldsymbol{k_\eta}\boldsymbol{a_\eta}\boldsymbol{b_\eta}\boldsymbol{e_\eta} + \boldsymbol{e_\eta}^\top(\boldsymbol{k_\eta}^2 - (\boldsymbol{a_\eta} + \boldsymbol{b_\eta})\boldsymbol{k_\eta} \\ &\quad - \boldsymbol{a_\eta}\boldsymbol{b_\eta} + k_2\boldsymbol{I})\boldsymbol{e_{\dot{\eta}}} - \boldsymbol{e_{\dot{\eta}}}^\top(\boldsymbol{a_\eta} + \boldsymbol{b_\eta} - \boldsymbol{k_\eta})\boldsymbol{e_{\dot{\eta}}}.\end{aligned}$$

Substituting (20) and (24) into above equation, we have

$$\begin{aligned}\dot{V}_t \leq &- k_1\lambda_{\dot{\xi}}\|\boldsymbol{e_{\dot{\xi}}}\|^2 + k_1\frac{\partial V_{\dot{\xi}}}{\partial \boldsymbol{e_{\dot{\xi}}}}[\dot{\boldsymbol{e}}_{\dot{\xi}}(\boldsymbol{e_{\dot{\xi}}}, \boldsymbol{e_{F\xi}}) - \dot{\boldsymbol{e}}_{\dot{\xi}}(\boldsymbol{e_{\dot{\xi}}}, 0)] \\ &- \boldsymbol{e_\eta}^\top\boldsymbol{k_\eta}\boldsymbol{a_\eta}\boldsymbol{b_\eta}\boldsymbol{e_\eta} - \boldsymbol{e_{\dot{\eta}}}^\top(\boldsymbol{a_\eta} + \boldsymbol{b_\eta} - \boldsymbol{k_\eta})\boldsymbol{e_{\dot{\eta}}}.\end{aligned} \tag{26}$$

According to (17), $\dot{\boldsymbol{e}}_{\dot{\xi}}(\boldsymbol{e_{\dot{\xi}}}, \boldsymbol{e_{F\xi}})$ is Lipschitz with respect to $\boldsymbol{e_{F\xi}}$. Considering the response speed of the rotors and the servos is fast, we assume the force $\boldsymbol{F}$ in (21) can be tracked all the time, and for bounded $\boldsymbol{F}$ θ, and ψ, $\boldsymbol{e_{F\xi}}$ defined in (16) can be expressed as $\boldsymbol{e_{F\xi}}(e_\phi, \boldsymbol{F}, \theta, \psi)$. It is easy to prove that $\boldsymbol{e_{F\xi}}$ is Lipschitz with respect to e_ϕ. Thus, $\dot{\boldsymbol{e}}_{\dot{\xi}}(\boldsymbol{e_{\dot{\xi}}}, \boldsymbol{e_{F\xi}}(e_\phi))$ is Lipschitz with respect to e_ϕ,

$$\|\dot{\boldsymbol{e}}_{\dot{\xi}}(\boldsymbol{e_{\dot{\xi}}}, \boldsymbol{e_{F\xi}}(e_\phi)) - \dot{\boldsymbol{e}}_{\dot{\xi}}(\boldsymbol{e_{\dot{\xi}}}, 0)\| \leq L|e_\phi|, \tag{27}$$

where L is a positive constant. According to the definitions in (7), we have $|e_\phi| \leq \|\boldsymbol{e_\eta}\|$. Then, substituting inequality (27) into (26), we have

$$\begin{aligned}\dot{V}_t \leq &- k_1\lambda_{\dot{\xi}}\|\boldsymbol{e_{\dot{\xi}}}\|^2 + k_1 L\|\boldsymbol{e_{\dot{\xi}}}\|\|\boldsymbol{e_\eta}\| - \lambda_\eta^{'}\boldsymbol{e_\eta}^\top\boldsymbol{e_\eta} \\ &- \boldsymbol{e_{\dot{\eta}}}^\top(\boldsymbol{a_\eta} + \boldsymbol{b_\eta} - \boldsymbol{k_\eta})\boldsymbol{e_{\dot{\eta}}},\end{aligned} \tag{28}$$

where $\lambda_\eta^{'} = \lambda_{min}(\boldsymbol{k_\eta}\ \boldsymbol{a_\eta}\ \boldsymbol{b_\eta})$. Defining $\boldsymbol{Q} \triangleq \begin{bmatrix} 2\lambda_{\boldsymbol{\xi}} & -\sqrt{k_1}L \\ -\sqrt{k_1}L & \lambda_\eta^{'} \end{bmatrix}$, (28) is rewritten as

$$\dot{V}_t \leq -\left[\frac{\sqrt{2k_1}}{2}\|\boldsymbol{e_\xi}\|\frac{\sqrt{2}}{2}\|\boldsymbol{e_\eta}\|\right]\boldsymbol{Q}\left[\frac{\sqrt{2k_1}}{2}\|\boldsymbol{e_\xi}\|\frac{\sqrt{2}}{2}\|\boldsymbol{e_\eta}\|\right]^\top - \boldsymbol{e_{\dot\eta}}^\top(\boldsymbol{a_\eta}+\boldsymbol{b_\eta}-\boldsymbol{k_\eta})\boldsymbol{e_{\dot\eta}}.$$

Recalling the upper bound of k_1 in (25), $\boldsymbol{Q}$ is positive definite and $\lambda_{min}(\boldsymbol{Q}) > 0$, which implies that the time derivative $\dot{V}_t$ is bounded by

$$\dot{V}_t \leq -\lambda_{min}(\boldsymbol{Q})(k_1\|\boldsymbol{e_\xi}\|^2/2 + \|\boldsymbol{e_\eta}\|^2/2) - \boldsymbol{e_{\dot\eta}}^\top(\boldsymbol{a_\eta}+\boldsymbol{b_\eta}-\boldsymbol{k_\eta})\boldsymbol{e_{\dot\eta}}.$$

According to the definition in (24), $\boldsymbol{a_\eta}+\boldsymbol{b_\eta}-\boldsymbol{k_\eta}$ is positive definite. Consequently, the zero equilibria of the errors $\boldsymbol{e_\xi}$ and $\boldsymbol{e_\eta}$ are locally asymptotically stable. □

4. SIMULATION AND EXPERIMENTAL VALIDATIONS

In this section, simulations are carried out in Matlab/SimMechanics environment to validate the effectiveness of the proposed control strategy for CTRUAV system. Then, the proposed control strategy is embed into the real CTRUAV system and a real flight experiments are implemented outdoors.

The drag force coefficients in (6) are obtained in a wind tunnel by the measuring method proposed in the previous work [22] and listed as $D_{xb} = 0.0242$, $D_{yb} = 0.0316$, $D_{zb} = 0.0546$. The influence of drag torque on the control performance is not obvious, the drag torque coefficients are given approximately as $D_{wx} = 0.01$, $D_{wy} = 0.01$, $D_{wz} = 0.005$.

4.1. Simulation results

In the simulations, the CTRUAV tracks the desired velocities and attitudes. For the sake of comparison, the PID controller and sliding-mode controller (SMC) [26] is implemented to deal with the same control tasks. The control parameters of the PID controller are obtained by particle swarm optimization algorithm [27]. In the simulation, the CTRUAV firstly takes off and climbs at the velocity of $\dot{z} = -1$ m/s. In the climbing process, the CTRUAV firstly tilts its coaxial rotors forward and tracks the speed of $\dot{x} = 3$ m/s at 2 s, and then rolls the fuselage and moves laterally at the speed of $\dot{y} = 2$ m/s at 5 s, and maintains the altitude as 7s. Next, yaw motion is performed by adjusting the tilt angles at 9 s, and pitch motion is carried out by adjusting the tilt angles and rotors' thrusts at 12 s. The control parameters of the proposed controller in the simulations are given as $a_\phi = 6$, $a_\theta = 5$, $a_\psi = 3$, $b_\phi = 6$, $b_\theta = 4$, $b_\psi = 3$, $k_{\dot{x}} = 3.7$, $k_{\dot{y}} = 3.2$, and $k_{\dot{z}} = 6.5$.

Table 2. Comparison of simulation results between the designed controller, PID and SMC.

	Rise times (s)	Settling times (s)	Maximum overshoot	Rise times (s)	Settling times (s)	Maximum overshoot
	Designed			PID		
θ	0.245	**0.37**	3.33%	0.431	0.602	**1.33**%
ψ	**0.281**	**0.45**	2.5%	3.64	0.565	2.95%
$\dot{x}$	**0.405**	**0.613**	4.33%	0.406	0.623	2.5%
$\dot{y}$	0.484	**0.767**	4.65%	**0.44**	1.184	7.51%
$\dot{z}$	0.36	0.582	2.35%	1.84	2.2	**0**%
	SMC					
θ	**0.2**	0.42	9%			
ψ	0.31	0.465	**1.2**%			
$\dot{x}$	0.428	0.639	**4.3**%			
$\dot{y}$	0.542	0.883	**3.2**%			
$\dot{z}$	**0.309**	**0.498**	3.3%			

The simulation results are depicted in Fig. 6. It is found that the proposed control strategy manages to achieve the attitude and velocity tracking for step control inputs $\dot{x}_d$, $\dot{y}_d$, $\dot{z}_d$, θ_d, and ψ_d, and stabilize ϕ. From Fig. 6(a), it is found that the settling time of the proposed controller is shorter than that of the PID controller and the SMC. In Fig. 6(b), the convergence speed of the proposed controller is faster than that of the PID controller and SMC in $\dot{x}$ and $\dot{y}$, and slower than that of the SMC in $\dot{z}$. However, in $\dot{x}$ and $\dot{y}$, the dynamic performance of the proposed controller is close with that of the PID controller and SMC, this is reasonable for the inherent dynamic characteristics of the CTRUAV. The rotors' rotational speeds and the tilt angles are illustrated in Figs. 6(c) and 6(d), respectively. Snapshots from the simulation test are presented in Fig. 6(e).

Moreover, in order to make quantitative comparisons of the controllers, some performance indexes are presented in Table 2. The rise time and the settling time of the proposed control strategy are less than that of PID and SMC, e.g. the rise time 0.281 of the designed controller is 77.2% of that of the PID and 90.6% of that of the SMC in ψ, the settling time 0.767 of the designed controller is 64.8% of that of the PID and 86.9% of that of the SMC in $\dot{y}$. On the other hand, in direction $\dot{y}$, the maximum overshoot 4.65% of the proposed controller is less than 61.9% of that of the PID controller. Although, the maximun overshoot of the SMC is smaller that of the designed controller, there exist obvious vibrations in different directions if the SMC is applied to control the CTRUAV, e.g. from Fig. 6(b), it is found that the error of the SMC is up to $[-0.024\ 0.032]$ m/s from 8 s to 12 s in direction $\dot{y}$. Hence, the performance of the proposed controller has been verified.

Remark 2: There exist various method in control gain selections, such as the particle swarm optimization algo-

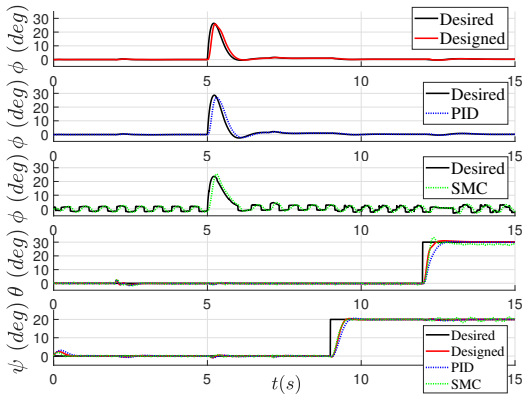

(a) Attitudes of CTRUAV.

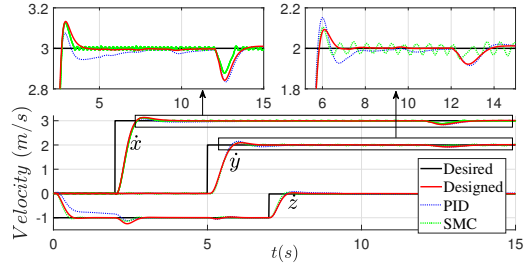

(b) Velocities of CTRUAV.

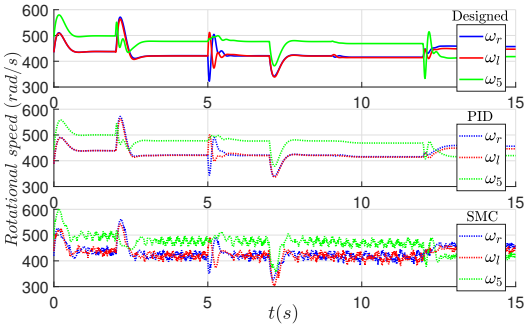

(c) Rotational speeds of rotors.

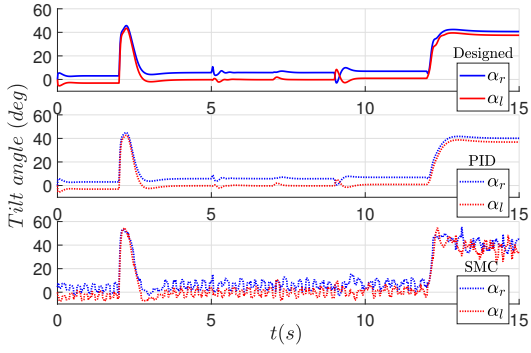

(d) Tilt angles.

(e) Simulational flight snapshots of CTRUAV.

Fig. 6. Simulation results of multidirectional maneuver.

rithm [28], the gain selection rules proposed in [29] and so on. In this work, the control gains of the proposed nonlinear controller are selected by the ergodic method accompany with manual parameter tuning method, and the objective function is the time integral of the squared state error

$$J_\eta = \int_0^\tau \boldsymbol{e_\eta}^\top \boldsymbol{e_\eta} dt, J_{\dot{\xi}} = \int_0^\tau \boldsymbol{e_{\dot{\xi}}}^\top \boldsymbol{e_{\dot{\xi}}} dt,$$

with tuning time τ,

4.2. Experimental results

To validate the effectiveness of the proposed control strategy for CTRUAV system, the real flight experiments have been carried out outdoors. The control parameters of the experiments are tuned based on that of the simulation and given as $a_\phi = 5$, $a_\theta = 4$, $a_\psi = 2.5$, $b_\phi = 4$, $b_\theta = 4$, $b_\psi = 2.5$, $k_{\dot{x}} = 3$, $k_{\dot{y}} = 3$, and $k_{\dot{z}} = 7$. Although they are slightly different from those used in the simulations, it is also meaningful, because tuning parameters based on that in the simulations can greatly reduced the crash risk and the time of tuning parameters in real-flight tests.

In the experiment with the proposed nonlinear cascade controller, as shown in Fig. 7, the CTRUAV firstly takes off at 5 s and moves forward at 16 s, then it moves to the right side laterally at 23 s, performs yaw motion at 30 s and moves forward at 31 s, it lands at 45 s at last. The rotors' rotational speeds and the tilt angles are illustrated in Figs. 7(c) and 7(d), respectively. From the experimental results, it is noticed that there is obvious attitude errors 3.4 deg and 3.9 deg in direction θ near 16 s and 33 s, respectively, when the CTRUAV is tilting the coaxial rotors and performing forward acceleration along direction $\dot{x}$. Furthermore, the state error in ϕ is within 4.2 deg while the CTRUAV is moving to the right side near 23 s. Snapshots from the real flight test by the proposed controller are presented in Fig. 7(e). For comparison, we also use the PID controller to perform similar flight experiment, and the experimental results are presented in Fig. 8. From Fig. 8(a), we can find that the max attitude error in direction θ reaches up to 10 deg near 32 s. From Fig. 8(b), we can find that the CTRUAV losts altitude while it is performing lateral movement near 23 s. The Root Mean Squard Errors (RMSEs) of the flight tests are defined as follows:

$$\mathfrak{x}_{RMSE}(t_0,t_1) = \sqrt{\left(\int_{t_0}^{t_1} (\mathfrak{x}_d(t) - \mathfrak{x}(t))^2 dt\right)/(t_1 - t_0)},$$

where $\mathfrak{x} = \dot{x}$, $\dot{y}$, $\dot{z}$, ϕ, θ, ψ. Then, the RMSEs of the whole flight test with proposed nonlinear cascade controller are $\dot{x}_{RMSE}(5,45) = 0.385$ m/s, $\dot{y}_{RMSE}(5,45) = 0.332$ m/s, $\dot{z}_{RMSE}(5,45) = 0.587$ m/s, $\phi_{RMSE}(5,45) = 1.273$ deg, $\theta_{RMSE}(5,45) = 1.222$ deg, $\psi_{RMSE}(5,45) = 16.886$ deg, and the RMSEs of the whole flight test with PID controller are $\dot{x}_{RMSE}(5,45) = 1.249$ m/s, $\dot{y}_{RMSE}(5,45) = 0.563$

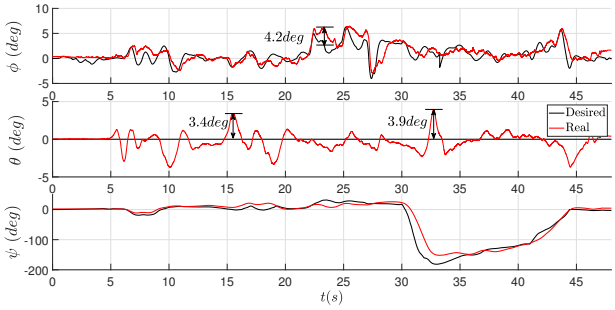

(a) Attitudes of CTRUAV.

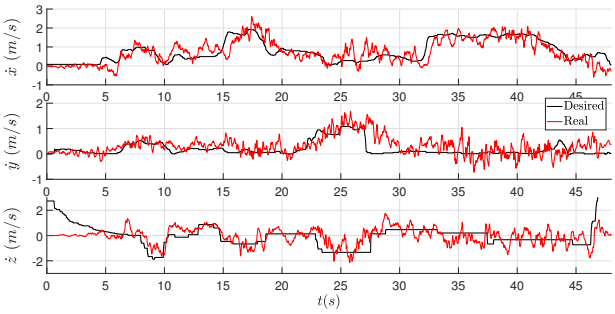

(b) Velocity of CTRUAV.

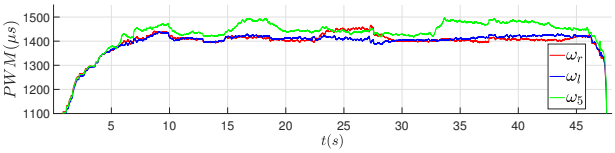

(c) Control signals of ESCs.

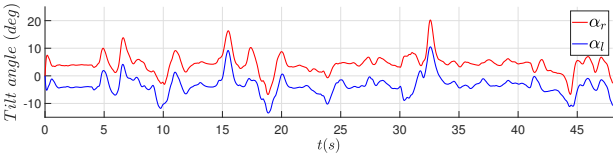

(d) Tilt angles.

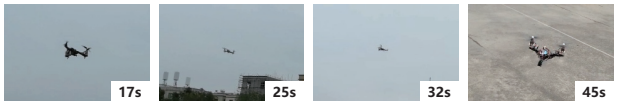

(e) Experimental flight snapshots of CTRUAV.

Fig. 7. Experimental results of CTRUAV (by proposed controller).

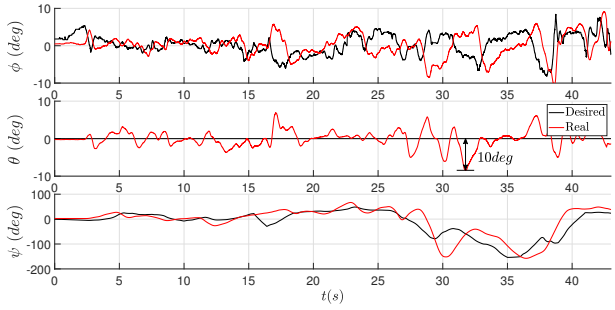

(a) Attitudes of CTRUAV.

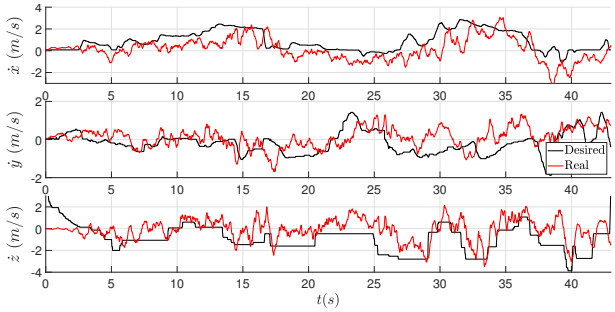

(b) Velocity of CTRUAV.

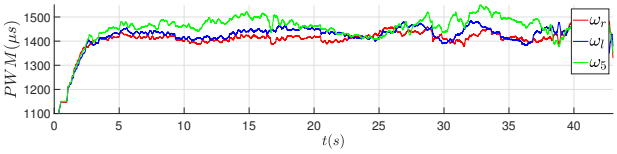

(c) Control signals of ESCs.

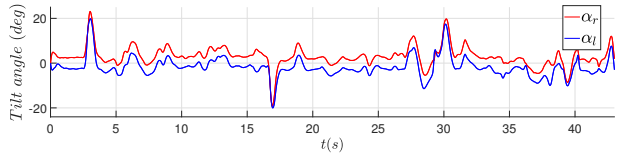

(d) Tilt angles.

Fig. 8. Experimental results of CTRUAV (by PID controller).

m/s, $\dot{z}_{RMSE}(5,45) = 1.741$ m/s, $\phi_{RMSE}(5,45) = 17.093$ deg, $\theta_{RMSE}(5,45) = 13.793$ deg, $\psi_{RMSE}(5,45) = 115.7$ deg. The RMSEs of the flight test with PID controller is significantly greater than that of the flight test with proposed nonlinear cascade controller, which means that the control accuracy of the proposed nonlinear cascade controller is better than that of the PID controller. From the experimental results, the CTRUAV successfully performs various maneuvers and tracks the desired velocity and attitude by the proposed controller, and the control performance of the proposed controller is better than that of the PID controller. A video showcasing is accompanied: https://youtu.be/pYLZne_WqoM.

5. CONCLUSION AND FUTURE WORK

In this paper, a cascade controller is proposed to realize the motion control for the CTRUAV, and the exponential stability of the resulting closed-loop CTRUAV system is proved. To validate the effectiveness of the proposed control strategy for CTRUAV system, the simulations and real flight experiments are performed. However, the proposed CTRUAV has some limitations, such as lacking consideration of exogenous disturbance, model inaccuracy, and component failures. These limitations are related to adaptive, robustness, and fault-tolerant control problems, which will be solved in our future work.

REFERENCES

[1] Y.-C. Choi and H.-S. Ahn, "Nonlinear control of quadrotor for point tracking: Actual implementation and experimental tests," *IEEE/ASME Transactions on Mechatronics*, vol. 20, no. 3, pp. 1179-1192, 2015.

[2] Y. Wu, K. Hu, X.-M. Sun, and Y. Ma, "Nonlinear control of quadrotor for fault tolerance: A total failure of one actuator," *IEEE Ttransactions on Systems, Man, and Cybernetics: Systems*, vol. 51, no. 5, pp. 2810-2820, 2021.

[3] A.-W. A. Saif, A. Aliyu, M. Al Dhaifallah, and M. Elshafei, "Decentralized backstepping control of a quadrotor with tilted-rotor under wind gusts," *International Journal of Control, Automation, and Systems*, vol. 16, no. 5, pp. 2458-2472, 2018.

[4] E. Cetinsoy, S. Dikyar, C. Hançer, K. Oner, E. Sirimoglu, M. Unel, and M. Aksit, "Design and construction of a novel quad tilt-wing UAV," *Mechatronics*, vol. 22, no. 6, pp. 723-745, 2012.

[5] F. Chen, R. Jiang, K. Zhang, B. Jiang, and G. Tao, "Robust backstepping sliding-mode control and observer-based fault estimation for a quadrotor UAV," *IEEE Transactions on Industrial Electronics*, vol. 63, no. 8, pp. 5044-5056, 2016.

[6] Y. Song and H. Wang, "Design of flight control system for a small unmanned tilt rotor aircraft," *Chinese Journal of Aeronautics*, vol. 22, no. 3, pp. 250-256, 2009.

[7] Z. Liu, Y. He, L. Yang, and J. Han, "Control techniques of tilt rotor unmanned aerial vehicle systems: A review," *Chinese Journal of Aeronautics*, vol. 30, no. 1, pp. 135-148, 2017.

[8] R. Donadel, G. V. Raffo, and L. Becker, "Modeling and control of a tiltrotor uav for path tracking," *IFAC Proceedings Volumes*, vol. 47, no. 3, pp. 3839-3844, 2014.

[9] D. N. Cardoso, S. Esteban, and G. V. Raffo, "A new robust adaptive mixing control for trajectory tracking with improved forward flight of a tilt-rotor UAV," *ISA Transactions*, vol. 110, pp. 86-104, 2021.

[10] E. D'Amato, G. Di Francesco, I. Notaro, G. Tartaglione, and M. Mattei, "Nonlinear dynamic inversion and neural networks for a tilt tri-rotor UAV," *IFAC-PapersOnLine*, vol. 48, no. 9, pp. 162-167, 2015.

[11] D. A. Ta, I. Fantoni, and R. Lozano, "Modeling and control of a tilt tri-rotor airplane," *Proc. of American Control Conference (ACC)*, IEEE, pp. 131-136, 2012.

[12] Z. Lv, Y. Wu, Q. Zhao, and X.-M. Sun, "Design and control of a novel coaxial tilt-rotor uav," *IEEE Transactions on Industrial Electronics*, vol. 69, no. 4, pp. 3810-3821, 2022.

[13] C. Papachristos and A. Tzes, "Modeling and control simulation of an unmanned tilt tri-rotor aerial vehicle," *Proc. of IEEE International Conference on Industrial Technology*, IEEE, pp. 840-845, 2012.

[14] S. Sridhar, G. Gupta, R. Kumar, M. Kumar, and K. Cohen, "Tilt-rotor quadcopter xplored: Hardware based dynamics, smart sliding mode controller, attitude hold & wind disturbance scenarios," *Proc. of American Control Conference (ACC)*, IEEE, pp. 2005-2010, 2019.

[15] B. Xian and W. Hao, "Nonlinear robust fault-tolerant control of the tilt trirotor UAV under rear servo's stuck fault: Theory and experiments," *IEEE Transactions on Industrial Informatics*, vol. 15, no. 4, pp. 2158-2166, 2018.

[16] A. B. Chowdhury, A. Kulhare, and G. Raina, "Backstepping control strategy for stabilization of a tilt-rotor UAV," *Proc of 24th Chinese Control and Decision Conference (CCDC)*, IEEE, pp. 3475-3480, 2012.

[17] J. R. Ahlquist, J. M. Carre no, H. Climent, R. de Diego, and J. de Alba, "Assessment of nonlinear structural response in a400m GVT," *Structural Dynamics*, vol. 3, pp. 1147-1155, Springer, 2011.

[18] J. Vorst, P. Booij, J. Brugman, D. Jeon, H. Choi, and H. Jun, "Kamov KA32T helicopter flight testing for training simulator development," 2009.

[19] M.-D. Hua, T. Hamel, P. Morin, and C. Samson, "Introduction to feedback control of underactuated vtolvehicles: A review of basic control design ideas and principles," *IEEE Control Systems Magazine*, vol. 33, no. 1, pp. 61-75, 2013.

[20] M. Allenspach, K. Bodie, M. Brunner, L. Rinsoz, Z. Taylor, M. Kamel, R. Siegwart, and J. Nieto, "Design and optimal control of a tiltrotor micro-aerial vehicle for efficient omnidirectional flight," *The International Journal of Robotics Research*, vol. 39, no. 10-11, pp. 1305-1325, 2020.

[21] O. M. A. Hafez, M. A. Jaradat, and K. S. Hatamleh, "Stable under-actuated manipulator design for mobile manipulating unmanned aerial vehicle (MM-UAV)," *Proc. of 7th International Conference on Modeling, Simulation, and Applied Optimization (ICMSAO)*, IEEE, pp. 1-6, 2017.

[22] Z. Lv, Y. Wu, and W. Rui, "Nonlinear motion control for a quadrotor transporting a cable-suspended payload," *IEEE Transactions on Vehicular Technology*, vol. 69, no. 8, pp. 8192-8206, 2020.

[23] V. I. Arnol'd, *Mathematical Methods of Classical Mechanics*, vol. 60, Springer Science & Business Media, 2013.

[24] T. Madani and A. Benallegue, "Backstepping control for a quadrotor helicopter," *Proc. of IEEE/RSJ International Conference on Intelligent Robots and Systems*, IEEE, pp. 3255-3260, 2006.

[25] T. Yang, N. Sun, and Y. Fang, "Adaptive fuzzy control for a class of MIMO underactuated systems with plant uncertainties and actuator deadzones: Design and experiments," *IEEE Transactions on Cybernetics*, vol. 52, no. 8, pp. 8213-8226, 2022.

[26] W. Perruquetti and J.-P. Barbot, *Sliding Mode Control in Engineering*, CRC press, 2002.

[27] W. Wang, J. T. Zhang, and T. Y. Chai, "A survey of advanced pid parameter tuning methods," *Acta Automatica Sinica*, vol. 26, no. 3, pp. 347-355, 2000.

[28] Eberhart and Y. Shi, "Particle swarm optimization: Developments, applications and resources," *Proc. of the Congress on Evolutionary Computation*, IEEE, vol. 1, pp. 81-86, 2001.

[29] T. Yang, N. Sun, Y. Fang, X. Xin, and H. Chen, "New adaptive control methods for n-link robot manipulators with online gravity compensation: Design and experiments," *IEEE Transactions on Industrial Electronics*, vol. 69, no. 1, pp. 539-548, 2022.

Shengming Li was born in Hunan, China. He received his B.S. degree in automation engineering and his M.S. degree in communication and information system from Dalian University of Technology, Dalian, Liaoning Province, in 2009 and 2012, respectively. He is working toward a Ph.D. degree at School of Innovation and Entrepreneurship, Dalian University of Technology from 2015. He is currently a senior engineer at School of Innovation and Entrepreneurship, Dalian University of Technology. His current research interests include intelligent robot and machine learning.

Zongyang Lv received his M.S. degree in mechanical engineering from the Dalian University of Technology, Dalian, China, in 2015. From 2015 to 2016, he joined Huawei Technologies Company Ltd., Shenzhen, China. He is currently pursuing a Ph.D. degree at the School of Control Science and Engineering, Dalian University of Technology from 2017. His current research interests include nonlinear control theory, fixed-time control theory, and control applications in unmanned aerial vehicles.

Lin Feng received his B.S. and M.S. degrees in internal combustion engine, and a Ph.D. degree in mechanical design and theory from the Dalian University of Technology, China, in 1992, 1995, and 2004, respectively. He is currently a Professor and a Doctoral Supervisor with the School of Innovation Experiment, Dalian University of Technology. His research interests include intelligent image processing, robotics, data mining, and embedded systems.

Yuhu Wu received his Ph.D. degree in mathematics from the Harbin Institute of Technology, Harbin, China, in 2012. Since 2012, he has held an Assistant Professor position with the Harbin University of Science and Technology, Harbin. He held a Postdoctoral Research position with Sophia University, Tokyo, Japan, from 2012 to 2015. In 2015, he joined the School of Control Science and Engineering, Dalian University of Technology, Dalian, China, where he is currently a Full Professor. His research interests are related to optimization, and nonlinear control theory and applications of control to Boolean networks, automotive powertrain systems, and unmanned aerial vehicles.

Yingshun Li received her Ph.D. degree in pattern recognition and intelligent system from the Northeast University, Shenyang, China, in 2006. She held a Professor position with the Beijing Institute of Petrochemical Technology, Beijing, from 2015 to 2017. In 2017, she joined the School of Control Science and Engineering, Dalian University of Technology, Dalian, China, where she is currently a professor. Her research interests are related to the artificial intelligence, the fault diagnosis and health management of military equipment.